Nat. Hazards Earth Syst. Sci. Discuss., 2, 7807–7835, 2014
www.nat-hazards-earth-syst-sci-discuss.net/2/7807/2014/
doi:10.5194/nhessd-2-7807-2014


Natural Hazards and Earth System Sciences
Open Access
Discussions



# Earthquake-induced deformation estimation of earth dam by multitemporal SAR interferometry: the Mornos Dam case (Central Greece)

**S. Neokosmidis[1], P. Elias[2], I. Parcharidis[1], and P. Briole[3]**

[1]Harokopio University of Athens, Department of Geography, Athens, Greece
[2]National Observatory of Athens, Institute of Astronomy, Astrophysics, Space Applications and Remote Sensing, Athens, Greece
[3]Ecole Normale Superieure, Department of Geosciences, France

Received: 19 November 2014 – Accepted: 8 December 2014 – Published: 22 December 2014

Correspondence to: S. Neokosmidis (s.neokosmidis@noa.gr)

Published by Copernicus Publications on behalf of the European Geosciences Union.

## Abstract

The scope of this paper concerns the investigation of Mornos earth Dam (Central Greece) deformation induced by major earthquake events occur in the broader area. For this purpose multitemporal SAR interferometry method was used. Specifically, the technique of Differential Interferometry SBAS and for the time series analysis the Singular Value Decomposition algorithm were applied. The data used were ascending and descending acquisitions of AMI/ERS-1 & 2 and ASAR/ENVISAT scenes covering the period 1993–2010. Five very strong seismic events with epicenters close to the dam, at the same period, were consider as potential sources of deformation. Lake level changes were also considered as an additional factor of induced deformation. Results show a maximum deformation rate of 10 cm along the line of sight for the whole period. Although the observed deformation appears to be due to changes in water level following a particular pattern, there are discontinuous over time which coincide with specific seismic events.

## 1 Introduction

ams are multi-purpose projects having significant social and conomic impact, such as flood control, irrigation, water upply and electricity production. Monitoring a dam plays an ssential role in its management and operation, especially for nsafe conditions or problems that require appropriate orrective measures at the early stages. Possible failure can ause great disasters with enormous social, economic and cological costs (Dekay et al., 1992; James et al., 2000). The inematic behavior is directly related to the probability of ts failure, for this reason, its monitoring is of particular mportance.

During the last decades, remote sensing techniques (e.g. laser scanner, differential interferometry, etc.) came to complement the methods for measuring the displacement of infrastructures with in-situ instruments as GPS, etc. Among these techniques, the Differential Interferometry SAR (DInSAR) is used to measure the micro-movements





NHESSD
2, 7807–7835, 2014

with millimeter precision. In the previous years, in order to study the structural deformation of Mornos dam four survey campaigns from 2002–2004 were carried out (Gikas et al., 2005). In this paper the study of the surface deformation, occurring in the region of the Mornos dam and the dam itself which is based on the application of Differential Radar Interferometry and SVD (Singular Value Decomposition) methodologies are presented. Our study is focused on the period of 1992–2000 and 2003–2010, exploiting AMI/ERS-1 & 2 and ASAR/ENVISAT, ascending and descending acquisitions. The availability of these ascending/descending data set allows us to discriminate the vertical and East–West displacement components as well. The importance of the Mornos dam, being the provider of reservoir of potable water to the greater metropolitan area of Athens, supporting 4.5 million people daily along with the fact that it is located in a seismically active area was the motivation of the current study.

## 2 The test site

### 2.1 Geological setting

Mornos river with a total length of 77 km, crosses the central mainland Greece. The sources are located on the southern slopes of Oiti, descending towards the south draining the basin located between Giona, Vardousion and Lidoriki and flows into the limits of the Gulf of Corinth and Patras, west of Nafpaktos.

The artificial lake of Mornos (Fig. 1), 7 km west of Lidoriki was built to meet the ever growing needs for water supply of Athens. The total surface of the lake, which is the average level, is about 15.5 $km^2$ making it the ninth largest artificial lake in Greece.

The main geological formations of the area belong to the External Hellenides, namely the Parnassos-Giona, Vardousia and Pindos geotectonic units. The area in which the dam was constructed consists exclusively of flysch, formation of Pindos unity.

The right (north) dam's abutment is characterized by low-grade formations due to intense tectonism. In the left (south) abutment, dominated by sandstones (flysch sandstone phase) which are mainly medium-layered with thin intercalations of siltstone and are generally corrugated aspects of large-scale.

### 2.2 Dam description

The construction of Mornos Dam began in 1969. The dam is located in the Mornos River, about 220 km north-west of Athens and is one of the largest earthen dams in Europe. The repletion of the reservoir began in 1979 and all works were completed by 1981. It is a large earth dam with a medium size central clay core. It is 126 m high, the crest length is 815 m and its width from toe to toe is 660 m (Fig. 2). It forms a man-made reservoir with surface area of 18.5 $km^2$ and watershed area of 560 $km^2$. Its maximum capacity is 764 million $m^3$ of water, while its operational volume is 630 million $m^3$. With the installation of pumping units an additional 70 million $m^3$ of water can be abstracted. The embankment component aggregates, which vary in size from sand particles to gravels, consist mainly of sedimentary (limestone, sandstone and shale) rocks (Lahmeyer, 1976). The lake has a maximum depth exceeding 100 m and an average depth of 52 m (Papadimitrakis and Karalis, 2009). It consists of two sub-basins (Fig. 3) communicating through a narrow strait. Mornos River as well as a number of streams discharge into the Lake.

## 3 Seismic hazard of the broader area

In the surrounding area of the dam several seismic events over 5.0 $M_w$ (Fig. 4a and b) have occurred, within the temporal range covered by this study. Particularly:

### 3.1 The June 1995 Aigio earthquake

On 15 June 1995, an earthquake of moment magnitude 6.4 $M_w$ occurred in the western part of the Gulf of Corinth, Greece, (Fig. 4a) causing the loss of 26 human lives and inflicting considerable damage mainly in the northern part of Peloponnesus. The



Discussion Paper | Discussion Paper | Discussion Paper | Discussion Paper |
NHESSD
2, 7807–7835, 2014

earthquake was located according to the National Observatory of Athens about 12 km to the NNE of Aigion, under the northern coast of the Gulf and 23 km SSE of Mornos Lake. The Harvard solution (HRV, 1995) is an East–West striking, almost pure normal fault with a dip angle of 45° (Bernard et al., 1997).

### 3.2 The April 2007 Trichonis earthquake

During April 2007, a seismic swarm took place in the area of Trichonis Lake (W. Greece), 43 km West of Mornos Lake (Fig. 4a). The swarm began with small events, on 9 April and two days later the three strongest events of the entire sequence occurred, with sizes ranging from 5.0 to 5.2 $M_w$ located in the southeastern part of Trichonis Lake. The seismic activity continued for a month with smaller magnitude events (Evangelidis et al., 2008; Kiratzi et al., 2008). This seismic activity was not correlated with any of the two fault zones at the northern and southern edges of the lake but with two unmapped NNE–SSW and NW–SE faults along its eastern shore (Evangelidis et al., 2008; Kiratzi et al., 2008; Sokos et al., 2010a).

### 3.3 The June 2008 Movri earthquake

On 8 June 2008, an earthquake of 6.5 $M_w$ and depth 17.5 km struck NW Peloponnesus (Fig. 4a). The epicenter was located in the wider Andravida area (Movri), 30 km SW from the city of Patras and 82 km SW of Mornos lake. The horizontal deformation filed was extended even far away the epicenter (Serpetsidaki et al., 2014). According to the moment tensor solutions for the earthquake issued (NOA, HARV, INGV, USGS, ETHZ, AUTH) and the geographical distribution of its aftershocks, the fault strikes NE–SW, dips ~ 85° NW while the motion was right-lateral with small reverse component. (Papadopoulos et al., 2010). It was felt throughout Peloponnesus, in Western Greece and in Attica and especially in the city and the suburbs of Patras. It triggered a number of landslides and rockfalls, toppled old buildings and poorly reinforced houses and cracked reinforced concrete buildings in nearby communities. No evidence of surface rupture or significant surface deformation based on field work was observed (Briole et al., 2008).

### 3.4 The December 2008 Amfiklia earthquake

On the 13 December 2008, 08:27 GMT, an earthquake measuring 5.1 $M_w$ occurred at about 10 km SE of the town of Lamia in central Greece (Fig. 4a), close to the small town of Amfiklia and 40 km NE of Mornos Lake. Despite its moderate magnitude the earthquake caused minor damage (mostly cracks and plaster falls) in Amfiklia and nearby villages. Limited landslides were also observed and as a consequence traffic in one country road was interrupted for a few hours. Epicenters of this small sequence are gathered on top of the south facing slope of the topographic high to the north of Amfiklia. Known large faults have been mapped to the north and dip to the north. In this frame, the 2008 sequence appears to be related to a small, antithetic to the known large faults, structure that bounds the Gravia–Amfiklia depression to the north (Ganas and Papoulia, 2000; Roberts and Ganas, 2000).

### 3.5 The January 2010 Efpalion earthquake

On 18 January 2010, 15:56 UTC, an 5.1 $M_w$ (National Observatory of Athens; NOA) earthquake occurred near the town of Efpalion (western Gulf of Corinth, Greece) (Fig. 4a), about 10 km to the east of Nafpaktos, along the north coast of the Gulf and 20 km SSW of Mornos Dam. Another strong event occurred on 22 January 2010, 00:46 UTC with 5.1 $M_w$ (NOA) approximately 3 km to the NE of the first event. The two largest events were accompanied by a sequence of aftershocks which lasted almost six months. Both M5+ shocks exhibited normal faulting along ~ E–W trending planes. The first event ruptured a blind, north-dipping fault, accommodating north–south extension of the Western Gulf of Corinth. The dip direction of the second event is rather unclear, although a south dip plane is weakly imaged in the post-22 January 2010 aftershock distribution (Sokos et al., 2010b).





NHESSD
2, 7807–7835, 2014

Earthquake-induced deformation of Earth dam by SAR Interferometry

S. Neokosmidis et al.

## 4 SAR data used and interferometric processing

At the present work archived data from AMI (Active Microwave Instrument) and ASAR (Advanced Synthetic Aperture Radar) active sensors mounted on ERS-1 & 2 and ENVISAT satellites operated by European Space Agency (ESA) were exploited for the interferometric analysis.

A total number of 128 Single Look Complex (SLC) acquisitions of mode I2 (incidence angle ~ 23°), with VV polarization operating in C-band, covering an area of 100 km by 100 km were used. Among them, for the period 1992–2000, a number of 20 ascending and 40 descending acquisitions were acquired by AMI active sensor. Moreover, for the period of 2003–2010, a number of 29 ascending and 39 descending acquisitions were acquired from ASAR active sensor. High accuracy orbital data from DELFT Institute (NL) for Earth-Oriented Space Research (DEOS) (Scharoo and Visser, 1998) were obtained for ERS-1 & 2 satellites. Moreover, high accuracy orbital data from Doppler Orbitography and Radio-positioning Integrated by Satellite (DORIS) instrument were obtained for ENVISAT satellite. The topographic phase was simulated based on SRTM V3 DEM of approximate 90 m spatial resolution.

In order to relate the pattern of the deformation with possible sources of deformations, seismological data for the period 1992–2010 for the Mornos region and the wider area, which are available from the website of European Mediterranean Seismological Centre (EMSC) and the Institute of Geodynamics, National Observatory of Athens (NOA) as well as data of the water level of the Mornos artificial Lake given by the Athens Water Supply and Sewerage Company (EYDAP SA) were used.

In the present study we have applied the DInSAR technique, which is based on exploiting the phase difference (interferogram) between pairs of SAR observations acquired at different time slots; this allow us to extract information of the displacements projected to the radar Line Of Sight (Gabriel et al., 1989; Massonnet et al., 1993). Particularly, the Small Baseline Subset methodology (Berardino et al., 2002) that relies on an appropriate combination of the DInSAR interferograms by using subsequently acquired SAR data, was used. Moreover, to reveal the deformation history, Singular Value Decomposition (SVD) method was also applied (Berardino et al., 2002; Usai, 2002). The SVD method connects independent subsets of SAR acquisitions separated by large spatial baselines, thus increasing the number of data used for the analysis of the area of interest (Manzo et al., 2005). Gamma processing software was used for processing and manipulating SAR data (Wegmuller et al., 1998) ran at Linux operated system.

Two separate processing procedures were carried out for AMI and ASAR datasets. All the interferometric pairs were multilooked by a factor of 1 in range and 5 in azimuth direction. The data set was co-registered to a single master scene, obtaining co-registration accuracies for the slaves less than 0.06 pixels in range and 0.2 pixels in azimuth. A subset of the full image frame was selected, by cropping the co-registered scenes to the Area of Interest (AOI).

The topographic component was removed to produce the differential interferograms (referred as interferograms hereafter). The interferometric pairs are characterized by small spatial and temporal baselines in order to limit the noise components usually referred to as decorrelation phenomena (Zebker and Villasenor, 1992). For the period of AMI acquisitions (1992–2000), spatial perpendicular baselines up to 300 m and temporal baselines up to 3 years for the ascending as well as up to 250 m and up to 2 years for the descending track were selected to form a sufficient network. For the period of ASAR acquisitions (2003–2010), spatial perpendicular baselines up to 300 m and temporal baselines up to 3 years for the ascending as well as up to 300 m and up to 2 years for the descending track were selected (Fig. 5). Particularly, 41 AMI interferograms were produced from the ascending and 134 from the descending track. Moreover, 71 ASAR interferograms were produced from the ascending and 171 from the descending track. The interferograms were further analyzed and filtered using adaptive filters (Goldstein and Werner, 1998).

The interferograms were unwrapped using the minimum cost-flow algorithm (Constatini, 1998). The threshold for the average coherence was set to 0.3. The reference point





NHESSD
2, 7807–7835, 2014

was carefully selected in order to avoid biases which can lead to shifts in the deformation patterns. It was located on stable ground 7 km East–Northeast of the dam area, in Lidoriki village, near LIDO permanent GPS station from Corinth Rift Laboratory network – CRL (http://crlab.eu). The velocity of LIDO for east, north and up components is 11.3, 0.3 and −0.3 mm $yr^{-1}$ respectively (http://ngpros.space.noa.gr). The estimation of the temporal evolution of the deformation is calculated by using a weighted least-squares algorithm that minimizes the sum of squared weighted residual phases.

## 5 Interferometric results and temporal comparison with relevant seismic events

The final products were projected to Universal Transverse Mercator (UTM) projection and superimposed over the shaded relief.

Due to the fact that the sensor incidence angle is $\sim 23^{\circ}$ and the LOS vector is more sensitive to vertical displacement when we refer to uplifting/subsidence in single track solutions, we make the assumption that the direction of deformation is vertical. Moreover, negative velocities do not necessarily represent subsidence, but possibly slower rates towards the satellite respecting the reference point.

### 5.1 Temporal ground deformation for period 1992–2000, during AMI acquisitions

The deformation maps of ascending (Fig. 6a) and descending (Fig. 6b) tracks as well as the time series deformation measurements for specific points on the dam are presented herein.

In Fig. 6a it is indicated that generally the relative velocities towards and away from the satellite along the LOS, varied between maximum values of +10 and −10 mm $yr^{-1}$, respectively. Particularly, an area along the lake shore “A” across from Lidoriki village was uplifting 5 mm $yr^{-1}$ while higher to the mountain Vardousia a subsidence of 2 mm $yr^{-1}$ was measured. Moreover, there is an area at the Giona Mountain “B” that was subsiding up to 8 mm $yr^{-1}$ and perhaps it is due to landslide phenomena. Focusing on the dam the left – North abutment seem stable with a slight uplift towards the dam in the range of 2 mm $yr^{-1}$, while the right – South abutment and the upstream side of the dam were considered stable.

In Fig. 6b the relative velocities towards and away from the satellite along the LOS varied between maximum values of +12 and −12 mm $yr^{-1}$, respectively. Particularly an area along the foothills of Giona Mountain "A" remains stable but at higher altitudes an uplift of about 3 to 5 mm $yr^{-1}$ is observed. Moreover there is an area "B" at the Vardousia Mountain subsiding 4 to 6 mm $yr^{-1}$. Focusing on the area of the dam, both the abutments are characterised as stable with a small subsidence of 1 mm $yr^{-1}$ while the downstream side of the dam is subsiding 7 mm $yr^{-1}$.

Time series analysis diagrams by means of SVD for specific point targets (Fig. 7) on the downstream side of the dam were plotted (Fig. 8). We selected the downstream side because of the orientation (westward) and the more coherence pixel and this is because when the satellite travels in a descending orbit, views a target area looking westward (in right-looking mode).

In Fig. 8, the deformation pattern of all points is similar. However, the deformation rate is directly related to the level of the artificial lake. During specific time periods, where the level of the artificial lake is increasing, either because of rainfall or due to the water drained from Evinos dam, the (Mornos) dam was subsiding, while during periods where the level of the lake is reduced, the dam was uplifting. However, during the period from 3 June 1995 to 17 September 1995 (indicated by black circle) the dam was expected to remain stable due to the constant level of the lake but instead it presented a deformation of −3 cm overall. This effect was probably due to the strong Aigion earthquake (6.2 $M_w$) occurred on 15 June 1995 and may affected locally the response of the dam. The correlation between the level of the artificial lake and the deformation in the dam is about 0.66.





NHESSD
2, 7807–7835, 2014

### 5.2 Temporal ground deformation for period 2003–2010, during ASAR acquisitions

The deformation maps of ascending (Fig. 9a) and descending (Fig. 9b) tracks as well as the time series deformation measurements for specific points on the dam (Fig. 7) are presented herein.

In Fig. 9a, the relative vertical velocities towards and away from the satellite along its LOS, varied between maximum values of +6 and −9 $\mathrm{mm\,yr^{-1}}$, respectively. Particularly, there is an area along the lake shore "A" across from Lidoriki village uplifting 3 $\mathrm{mm\,yr^{-1}}$ while higher to the mountain Bardousia a subsidence of 1.5 $\mathrm{mm\,yr^{-1}}$ was measured. Furthermore, North for the Bardousia, there is an area "B" subsiding 7 to 9 $\mathrm{mm\,yr^{-1}}$. This may be due to landslides phenomena or neotectonic movements in the area. Focusing on the area of the dam we observed that along the left – North abutment a dissimilar deformation was existed with a subsidence rate of 1 $\mathrm{mm\,yr^{-1}}$ near the dam, at the middle of the abutment an uplift of 2.5 $\mathrm{mm\,yr^{-1}}$ and again a subsidence of 1 $\mathrm{mm\,yr^{-1}}$ at the end. This was probably due to the different geological formation which caused landslides phenomena. The right – South abutment was characterised as stable and the upstream side of the dam presented a subsidence of 2 $\mathrm{mm\,yr^{-1}}$.

In Fig. 9b the relative velocities towards and away from the satellite along its LOS, varied between maximum values of +10 and −12 $\mathrm{mm\,yr^{-1}}$, respectively. An area along the foothills of the Giona Mountain "A" was uplifted 2 $\mathrm{mm\,yr^{-1}}$ and in higher altitudes a subsidence of about up to 5 $\mathrm{mm\,yr^{-1}}$ was observed. This may be due to tropospheric phenomena. Focusing on the area of the dam the left – North abutment had the same deformation pattern as in ascending track while the right – South abutment was uplifting 2 $\mathrm{mm\,yr^{-1}}$. The downstream side of the dam presented an uplift of 4 $\mathrm{mm\,yr^{-1}}$.The deformation pattern was the same for all points (Fig. 10) and the deformation rate was related to the level of the artificial lake. In periods where the lake level is increasing, the dam was subsiding and during the decrease of the level of the lake, the dam was uplifting respectively. However, during specific periods this behavior did not taken place.





NHESSD
2, 7807–7835, 2014

From 11 February 2007 to 5 August 2007 (left dashed circle) and 22 December 2009 to 3 October 2010 (right dashed circle) the relationship of the deformation rate and the level of the lake was vice versa. This effect was probably due to strong earthquakes occurred on 10 April 2007 in Trichonis lake (5.2 $M_w$) and on 18 January 2010 in Efpalio (5.3 $M_w$). They may affected locally the response of the dam. A more remote and stronger earthquake occurred on 8 June 2008 in Movri (6.2 $M_w$) which did not affect the response of the dam. The correlation between the level of the artificial lake and the deformation in the dam is about 0.29.

### 5.3 Decomposition of LOS deformation

Due to the availability of both ascending and descending tracks, we could compute the east–west and vertical components as Manzo et al. (2005) proposed. This investigation is focused only in the Mornos dam, Fig. 11 explains the basic rationale of this procedure.

For simplicity it is assumed that both ascending and descending LOS directions, belong to the *East-z* plane. In the Fig. 11, $\vartheta$ is the look-angle which is assumed as the same for both ascending and descending track. It is well known that for ERS-1 & 2 and ENVISAT satellites the look-angle is almost equal to 23°. Moreover the reference point for both tracks was the same. Also, $P$ is the investigated point target "observed" from both ascending and descending passes and $d$ the displacement vector relevant to $P$ in the East-$z$ plane.

Based on simply geometric considerations, the east–west and vertical displacement components are retrieved by:

$$d_{\text{East}} \approx \frac{(d_{\text{LOS\_Desc}} - d_{\text{LOS\_Asc}})/2}{\sin(\theta)} \quad (1)$$

$$d_{Z} \approx \frac{(d_{\text{LOS\_Desc}} + d_{\text{LOS\_Asc}})/2}{\cos(\theta)} \quad (2)$$





NHESSD
2, 7807–7835, 2014

Earthquake-induced deformation of Earth dam by SAR Interferometry

S. Neokosmidis et al.

where, $d_{LOS\_Asc}$ and $d_{LOS\_Desc}$ correspond to two radar lines of sight (Manzon et al., 2005).

#### 5.3.1 Decomposition of LOS Deformation, for Period 2003–2010, during ASAR acquisitions

This section presents the combination of ascending and descending deformation maps of ASAR, in order to retrieve the vertical (Fig. 12a) and east–west (Fig. 12b) component. This period was chosen due to the fact that the amount of ASAR acquisitions were more than that of AMI/ERS (1993–2000) as well as that in this period the seismicity in the broader area was higher. Using Eqs. (1) and (2) the maps of UP and EAST component were created.

In Fig. 12a, the dam presents a uniform vertical deformation of about $-4\,\mathrm{mm\,yr^{-1}}$ while at left – North abutment there is an area where the vertical deformation is about $-7\,\mathrm{mm\,yr^{-1}}$ while the other part has the same rate as the dam. Probably, this area presents landslide phenomena. The same phenomena perhaps has the right – South abutment as the vertical deformation is about $-8\,\mathrm{mm\,yr^{-1}}$.

Finally, in Fig. 14b, the dam presents a uniform deformation of about $2\,\mathrm{mm\,yr^{-1}}$ to the West while the left – North abutment present a differential horizontal deformation. The section near the dam and the end have a deformation of about $2\,\mathrm{mm\,yr^{-1}}$ to the East while the middle part has a deformation of about $2\,\mathrm{mm\,yr^{-1}}$ to the West. The right – South abutment presents a horizontal deformation to the East as the dam.

## 6 Conclusions

Monitoring strategic structures is an activity of paramount importance. For structures such as dams which have a high exposure factor, continuous monitoring using satellite data may represent one of the main non-structural countermeasures for risk mitigation. In this research paper we have applied a DInSAR technique using both ERS-1 & 2 AMI and ENVISAT ASAR scenes in order to observe the surface deformation of the Mornos dam as well as the behavior of the dam in relation to possible sources of deformation such as seismic events and artificial lake level. Our results show that SAR interferometry allows mapping of very local displacements at the dam as well as displacements on a regional scale around the reservoir. Specifically the maximum variation of the deformation of dam for the period 1993–2000 are about 7 cm while for the period 2003–2010 are about 4 cm. As regards the deformation in the dam the behavior of the dam is affected mainly by the water level and secondary by specific seismic events. As far as the correlation between water level and deformation in the dam is concerned, in the AMI/ERS (1993–2000) period the correlation is 0.66 while in the ASAR/ENVISAT (2003–2010) period is 0.29. This difference is due to the fact that in the period 2003–2010 there were more seismic events which affected the correlation than the previous period. No differential deformation of the dam itself was observed, capable to raise the level of concern.

The new very high resolution SAR sensors as RADASAT-2, Cosmo-SkyMed but mainly TERRASAR-X and Sentinel-1A (because of more opportunities for data provision to the scientific community), with different incidence angles than the usual I2 mode of $\sim 23^{\circ}$ of AMI/ERS and ASAR/ENVISAT need to be used in order to assess better the deformation. Geodetic GPS measurements can be applied to validate and calibrate the results.

*Acknowledgements.* The authors would like to thank European Space Agency (ESA) for the AMI/ERS and ASAR/ENVISAT data through cat-1 6287 and Athens Water Supply and Sewerage Company (EYDAP SA) for the water level of the Mornos artificial lake data.

## References

Berardino, P., Fornaro, G., Lanari, R., and Sansosti, E.: A new algorithm for surface deformation monitoring based on small baseline differential SAR interferograms, IEEE T. Geosci. Remote, 40, 2375–2383, 2002.





NHESSD
2, 7807–7835, 2014

Earthquake-induced deformation of Earth dam by SAR Interferometry

S. Neokosmidis et al.

Bernard, P., Briole, P., Meyer, B., Lyon-Caen, H., Gomez, J.-M., Tiberi, C., Berge, C., Cattin, R., Hatzfeld, D., Lachet, C., Lebrun, B., Deschamps, A., Courboulex, F., Larroque, C., Rigo, A., Massonnet, D., Papadimitriou, P., Kassaras, J., Diagourtas, D., Makropoulos, K., Veis, G., Papazisi, E., Mitsakaki, C., Karakostas, V., Papadimitriou, E., Papanastassiou, D., Chouliaras, M., and Stavrakakis, G.: The Ms = 6.2, 15 June 1995 Aigion earthquake (Greece): evidence for low angle normal faulting in the Corinth rift, J. Seismol., 1, 131–150, 1997.
Briole, P., Armijo, R., Avallone, A., Bernard, P., Charara, R., Deschamps, A., Dimitrov, D., Elias, P., Grandin, R., Ilieva, M., Lambotte, S., Lyon-Caen, H., Meyer, B., Mouratidis, A., Nercessian, A., Papanastassiou, D., Ruegg, J. C., Sokos, E., and Sykioti, O.: Multidisciplinary stude of the 8 June 2008, $M_w = 6.4$ Andravida earthquake, 31 General Assembly, European Seismol. Commission (Abstract), Hersonissos, Crete, Greece, 7–12 September, 2008.
Constantini, M.: A novel phase unwrapping method based on networks programming, IEEE T. Geosci. Remote, 36, 813–821, 1998.
DeKay, L. M. and McClelland. H. G.: Predicting loss of life in cases of dam failure and flash flood, Risk Anal., 13, 193–205, 1993.
Evangelidis, P. A., Konstantinou, I. K., Melis, S. N., Charalambakis, M., and Stavrakakis, N. G.: Waveform relocation and focal mechanism analysis of an earthquake swarm in Trichonis Lake, Western Greece, B. Seismol. Soc. Am., 98, 2804–811, 2008.
Gabriel, A., Goldstein, R., and Zebker, H.: Mapping small elevation changes over large areas by differential radar interferometry, J. Geophys. Res.-Sol. Ea., 7, 9183–9191, 1989.
Ganas, A. and Papoulia, I.: High-resolution, digital mapping of the seismic hazard within the Gulf of Evia rift, Central Greece using normal fault segments as line sources, Nat. Hazards, 22, 203–223, 2000.
Gikas, V. and Sakellatiou, M.: Settlement analysis of the Mornos earth dam (Greece): evidence from numerical modeling and geodetic monitoring, Eng. Struct., 30, 3074–3081, 2008.
Gikas, V., Paradissis, D., Raptakis, K., and Antonatou, O.: Deformation studies of the dam of Mornos artificial lake via analysis of geodetic data FIG Working Week, FIG, Cairo (Egypt), 2005.
Goldstein, R. M. and Werner, C. L.: Radar interferogram filtering for geophysical applications, Geophys. Res. Lett., 25, 4035–4038, 1998.
James, E. E., Scudder, D. M., Johan, F. G., and Wilfrid, M., G.: Lessons from a dam failure, Ohio J. Science, 100, 121–131, 2000.





NHESSD
2, 7807–7835, 2014

Earthquake-induced deformation of Earth dam by SAR Interferometry

S. Neokosmidis et al.

Kiratzi, A., Sokos, E., Ganas, A., Tselentis, A., Benetatos, C., Roumelioti, Z., Serpetsidaki, A., Andriopoulos, G., Galanis, O., and Petrou, P.: The April 2007 earthquake swarm near Lake Trichonis and implications for active tectonics in western Greece, Tectonophysics, 452, 51–65, 2008.

Lahmeyer International Consulting Engineers: Mornos dam: 780 million $m^3$ reservoir for water supply to Athens area, Technical Report, Athens (Greece), 1976.

Manzo, M., Ricciardi, P. G., Casu, F., Ventura, G., Zeni, G., Borgstrom, S., Berardino, P., Del Gaudio, C., and Lanari, R.: Surface deformation analysis in the Ischia Island (Italy) based on spaceborne radar interferometry, J. Volcanol. Geoth. Res., 151, 399–416, 2005.

Massonnet, D., Rossi, M., Carmona, C., Adragna, F., Peltzer, G., Feigl, K., and Rabaute, T.: The displacement field of the Landers earthquake mapped by radar interferometry, Nature, 364, 139–142, 1993.

Papadimitrakis, I. A. and Karalis, S.: 3-D water quality simulations in Mornos reservoir, Global NEST J., 11, 298–307, 2009.

Papadopoulos, G., Karastathis, V., Kontoes, C., Charalampakis, M., Fokaefs, A., and Papoutsis, I.: Crustal deformation associated with east Mediterranean strike-slip earthquake: the 8 June 2008 Movri (NW Peloponnese), Greece, earthquake ($M_w$6.4), Tectonophysics, 492, 201–212, 2010.

Roberts, P. G. and Ganas, A.: Fault-slip directions in central and southern Greece measured from striated and corrugated fault planes: comparison with focal mechanism and geodesy data, J. Geophys. Res.-Solid Ea, 105, 23443–23462, 2000.

Scharoo, R. and Visser, P.: Precise orbit determination and gravity field improvement for the ERS satellites, J. Geophys. Res., 103, 8113–8127, 1998.

Serpetsidaki, A., Elias, P., Ilieva, M., Bernard, P., Briole, P., Deschamps, A., Lambotte, Lyon-Caen, H., Sokos, E., and Tselentis, A.: New constraints from seismology and geodesy on the $M_w = 6.4$ 2008 Movri (Greece) earthquake: evidence for a growing strike-slip fault system, Geophys. J. Int., 199, 1373–1386, 2014.

Sokos, E., Pikoulis, V. E., Psarakis, E. Z., and Lois, A.: The April 2007 swarm in trichonis lake using data from a microseismic network, Bulletin of the Geological Society of Greece 2010, in: Proceedings of the 12 International Congress, Patras, May, XLIII, 4–2183, 2010a.

Sokos, E., Zahradnik, J., Kiratzi, J., Jansky, J., Gallovic, F., Novotny, O., Kostelecky, J., Serpetsidaki A., and Tselentis, G.: The Jenuary 2010 Efpalio earthquake sequence in the western Corinth Gulf (Greece), Tectonophysics, 530–531, 299–309, 2010b.

Usai, S.: A least-squares approach for long-term monitoring of deformations with differential SAR interferometry, in: Proceedings of the IEEE International Geoscience and Remote Sensing Symposium (IGARSS 2002), Toronto (Canada), 24–28 June 2002, 2, 1247–1250, 2002.
Wegmuller, U., Werner, C.: Gamma SAR processor and interferometry software, European Space Agency, (Special Publication), 414 part 3, 1687–1692, 1998.
Zebker, H. A. and Villasenor, J.: Deccorelation in interferometric radar echoes, IEEE transaction on Geoscience and Remote Sensing, 30, 950–959, 1992.





NHESSD
2, 7807–7835, 2014
Earthquake-induced deformation of Earth dam by SAR Interferometry
S. Neokosmidis et al.

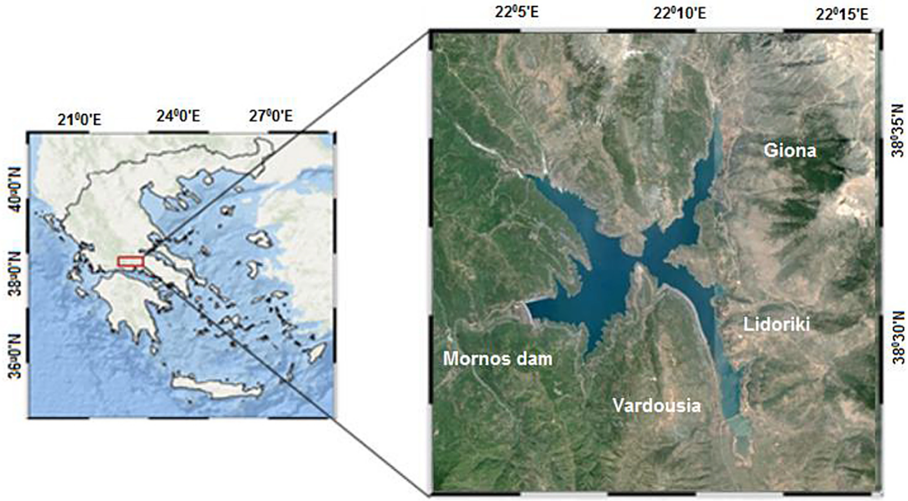


**Figure 1.** Location map of the study area.





NHESSD
2, 7807–7835, 2014

Earthquake-induced deformation of Earth dam by SAR Interferometry

S. Neokosmidis et al.

Title Page
Abstract | Introduction
Conclusions | References
Tables | Figures
◀I | ▶I
◀ | ▶
Back | Close
Full Screen / Esc
Printer-friendly Version
Interactive Discussion

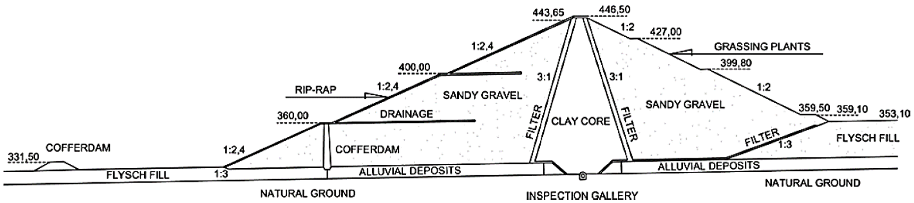


**Figure 2.** Cross section of Mornos Dam (Gikas et al., 2008).



NHESSD

2, 7807–7835, 2014

Earthquake-induced deformation of Earth dam by SAR Interferometry

S. Neokosmidis et al.

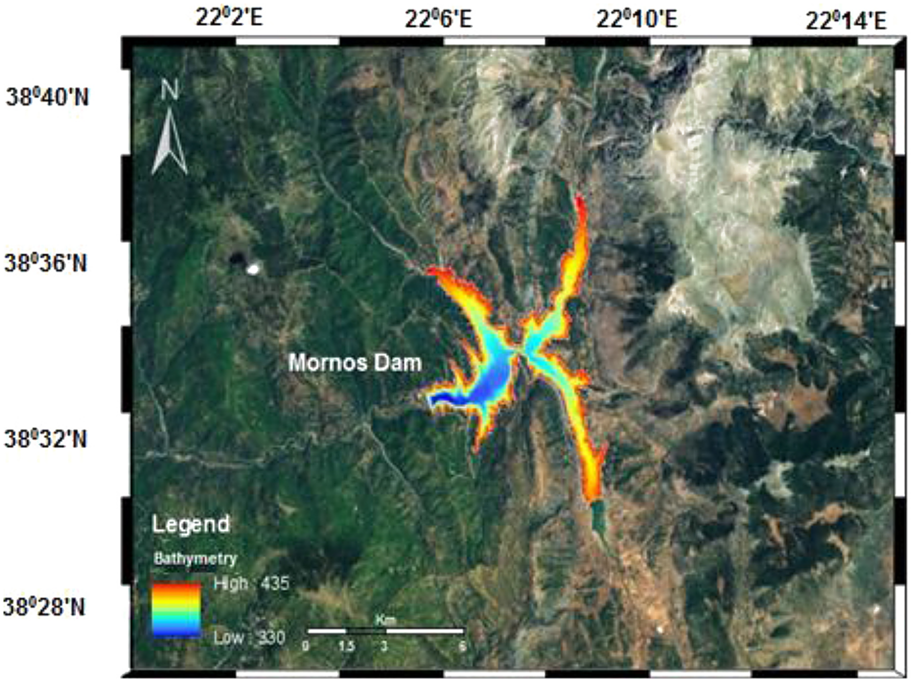


**Figure 3.** Location area and bathymetry of Mornos reservoir.





NHESSD

2, 7807–7835, 2014

Earthquake-induced deformation of Earth dam by SAR Interferometry

S. Neokosmidis et al.

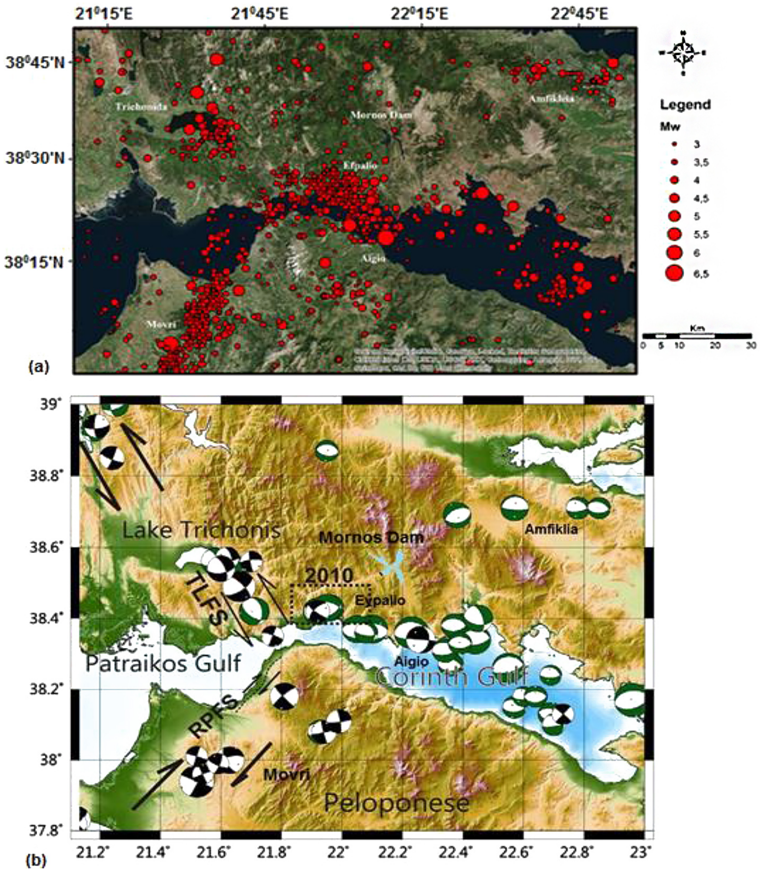


**Figure 4. (a)** Location of epicenters of the main seismic events in wide area (seismological data source: national Observatory of Athens). **(b)** Regional tectonic of wide area and available earthquake focal mechanisms (Sokos et al., 2010).





NHESSD
2, 7807–7835, 2014

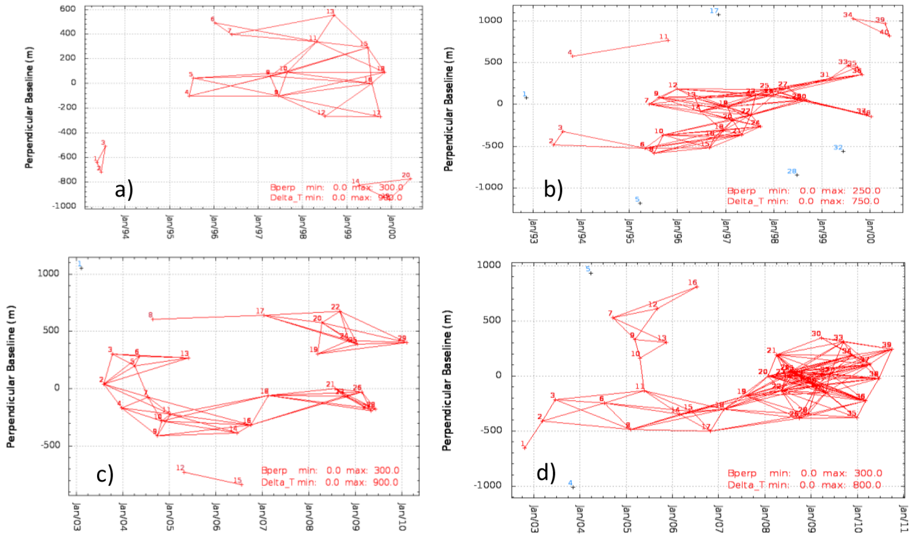


**Figure 5.** ERS scenes (Upper) and ENVISAT scenes (Down) networks. **(a)**, **(b)** Relate to the AMI ascending and descending dataset respectively and **(c)**, **(d)** relate to the ASAR ascending and descending dataset.



NHESSD

2, 7807–7835, 2014

**Earthquake-induced deformation of Earth dam by SAR Interferometry**

S. Neokosmidis et al.

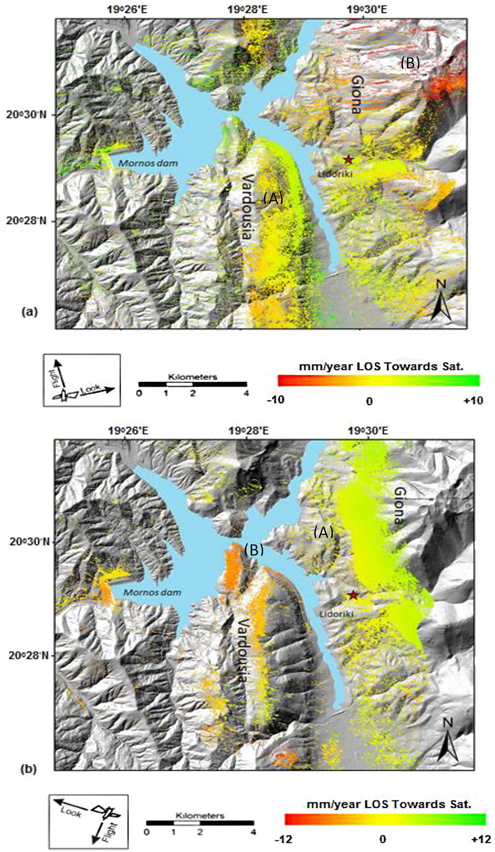


**Figure 6. (a)** SVD/SBAS LOS deformation rates from the period 1992–2000 (sensor AMI/ERS-1&2, ascending track). **(b)** SVD/SBAS LOS deformation rates from the period 1992–2000 (sensor AMI/ERS-1&2, descending track). The location of the reference point is shown with red star. Positive values represent deformation towards the satellite.





NHESSD
2, 7807–7835, 2014

Earthquake-induced deformation of Earth dam by SAR Interferometry

S. Neokosmidis et al.

Title Page
Abstract | Introduction
Conclusions | References
Tables | Figures
◄ | ►
◄ | ►
Back | Close
Full Screen / Esc
Printer-friendly Version
Interactive Discussion

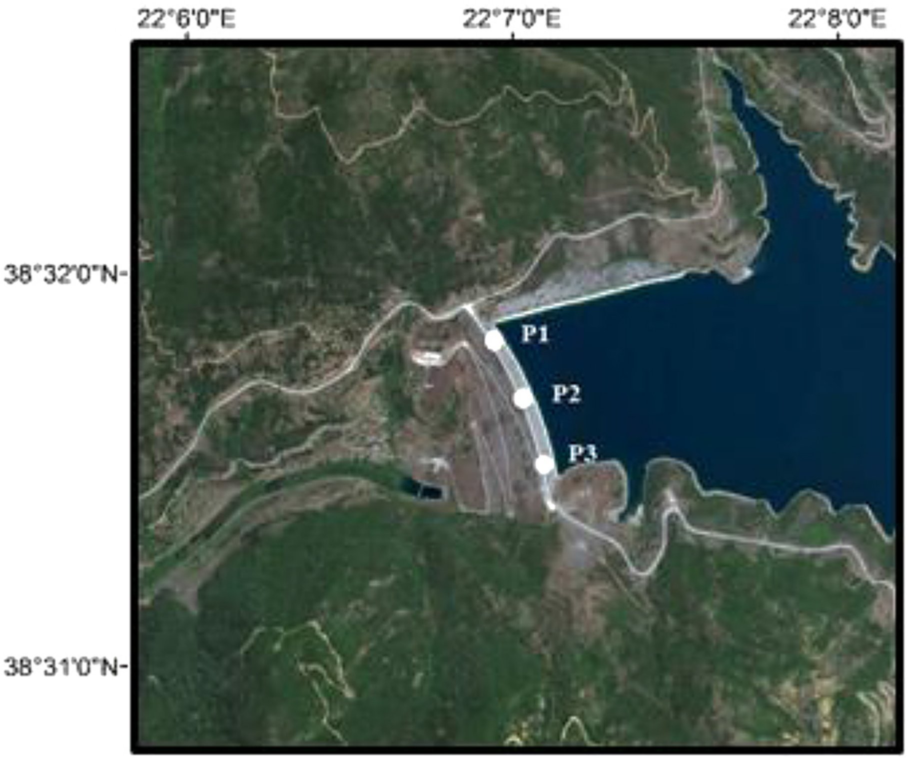


**Figure 7.** Selected point targets on the downstream side of the dam.





NHESSD
2, 7807–7835, 2014

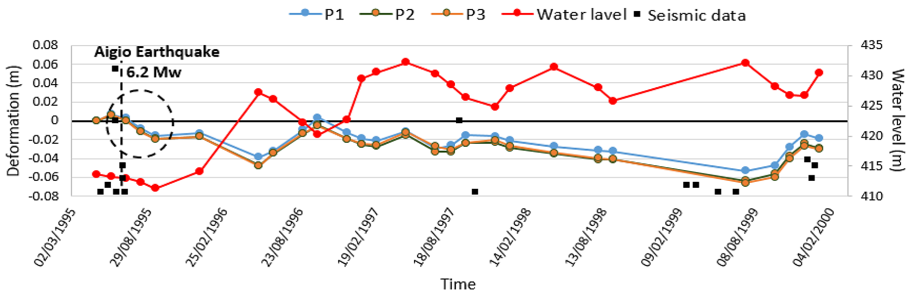


**Figure 8.** Correlation of time series deformation (1992–2000), level of artificial lake and seismic data for selected point targets on the Mornos dam.

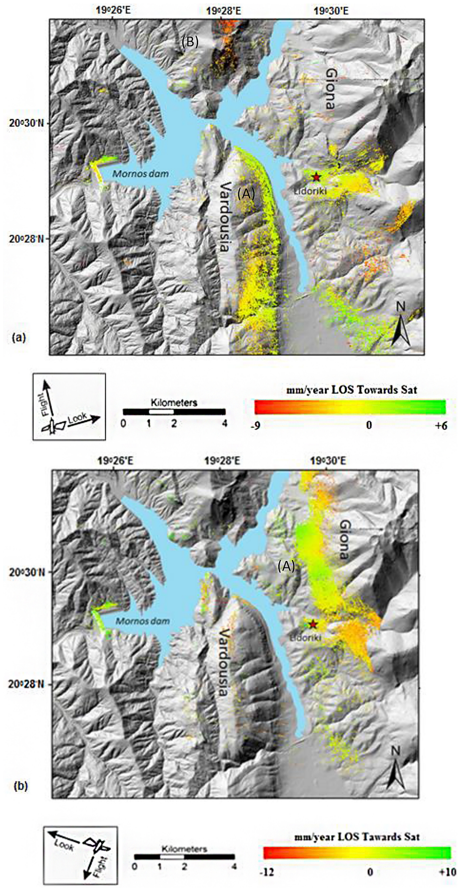


**Figure 9. (a)** SVD/SBAS LOS deformation rates from the period 2003–2010 (sensor ASAR/ENVISAT, ascending track). **(b)** SVD/SBAS LOS deformation rates from the period 2003–2010 (sensor ASAR/ENVISAT, descending track). The location of the reference point is shown with red star.



NHESSD

2, 7807–7835, 2014

Earthquake-induced deformation of Earth dam by SAR Interferometry

S. Neokosmidis et al.

Title Page
Abstract | Introduction
Conclusions | References
Tables | Figures
◀| |▶
◀ ▶
Back | Close
Full Screen / Esc
Printer-friendly Version
Interactive Discussion

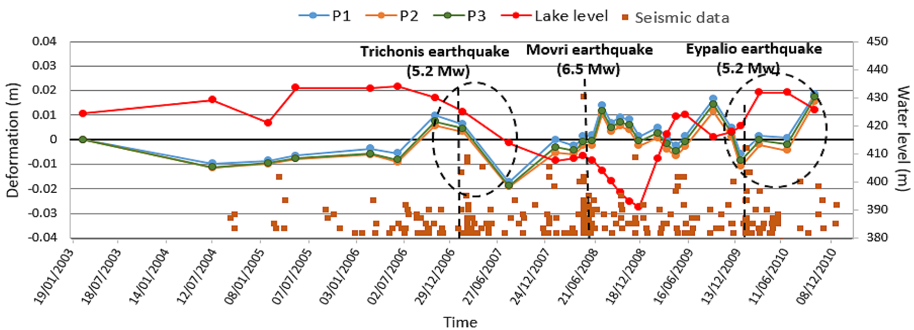


**Figure 10.** Correlation of time series deformation, level of artificial lake and seismic data at point targets on the Mornos dam.

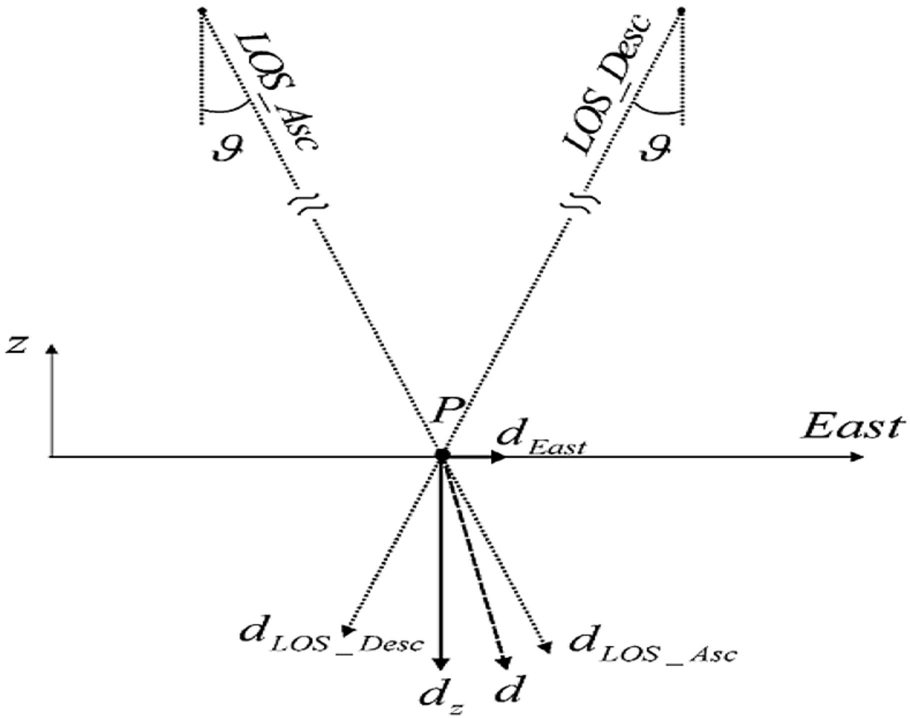


**Figure 11.** SAR geometry in the East-*z* plane with the displacement vector ***d*** (dashed line), its LOS projections dLOS_Asc and dLOS_Desc (dotted line) and the east–west and vertical deformation components dEast and dz (continuous line) highlighted, respectively. A simplified ascending and descending radar geometry is considered here, wherein we assume parallel satellite tracks, orthogonal to the East-*z* plane (Manzo et al., 2005).





NHESSD
2, 7807–7835, 2014

Earthquake-induced deformation of Earth dam by SAR Interferometry

S. Neokosmidis et al.

Title Page
Abstract | Introduction
Conclusions | References
Tables | Figures
◀| |▶
◀ ▶
Back | Close
Full Screen / Esc
Printer-friendly Version
Interactive Discussion

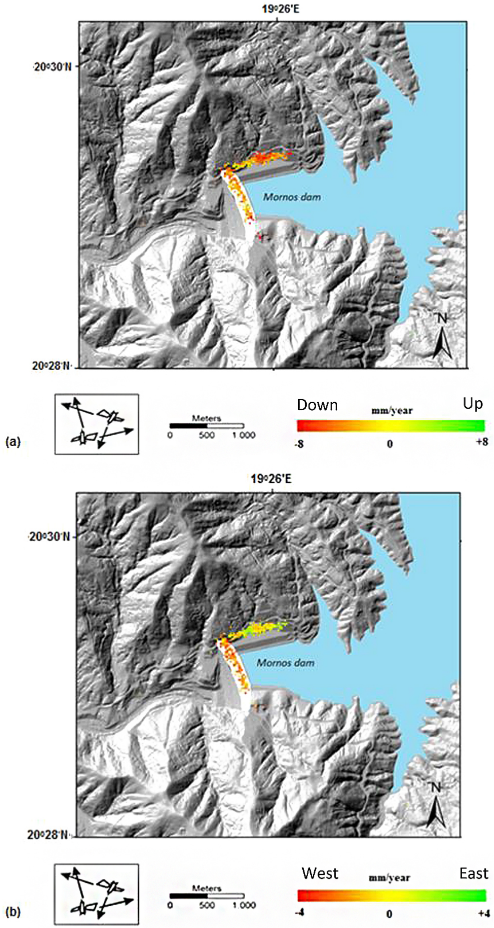


**Figure 12. (a)** SVD/SBAS UP component deformation rates from the period 2003–2010 (satellite ENVISAT). **(b)** SVD/SBAS EAST component deformation rates from the period 2003–2010 (satellite ENVISAT).





NHESSD
2, 7807–7835, 2014